Hyperspectral Uncertainty Quantification by Optimization

Hyperspectral Uncertainty Quantification by Optimization

Abdullah Abdulaziz*, Audrey Repetti*†, and Yves Wiaux*
*The school of Engineering and Physical Sciences, Edinburgh EH14 4AS, United Kingdom.
†The school of Mathematics and Computer Sciences, Edinburgh EH14 4AS, United Kingdom.

***Abstract*—We leverage convex optimization techniques to perform Bayesian uncertainty quantification (UQ) for hyperspectral (HS) inverse imaging problems. The proposed approach generalizes our recent work for single-channel UQ [1]. Similarly, the Bayesian hypothesis test is formulated as a convex minimization problem and solved using a primal-dual algorithm to quantify the uncertainty associated with particular 3D structures appearing in the maximum a posteriori (MAP) estimate of the HS cube. We investigate the interest of the proposed method for wideband radio-interferometric (RI) imaging that consists in inferring the wideband sky image from incomplete and noisy Fourier measurements. We showcase the performance of our approach on realistic simulations.**

I. Introduction

Many HS imaging problems, particularly in medicine and astronomy, consist in estimating an unknown cube, written in a matrix form as $\bar{\boldsymbol{X}} = (\bar{\boldsymbol{x}}_1, .., \bar{\boldsymbol{x}}_L) \in \mathbb{R}_+^{N\times L}$, from noisy and possibly incomplete measurements $\boldsymbol{Y} = (\boldsymbol{y}_1, .., \boldsymbol{y}_L) \in \mathbb{C}^{M\times L}$. Each column $\bar{\boldsymbol{x}}_l$ of the matrix $\bar{\boldsymbol{X}}$ represents a spectral channel and the column $\boldsymbol{y}_l$ represents the respective measurements. The full HS measurement model can be expressed as $\boldsymbol{Y} = \Phi(\bar{\boldsymbol{X}}) + \boldsymbol{W}$, where $\Phi(\bar{\boldsymbol{X}}) = ([\boldsymbol{\Phi}_l \bar{\boldsymbol{x}}_l]_{\forall l\in\{1,\dots L\}})$ is the HS measurement operator with $\boldsymbol{\Phi}_l$ being the measurement matrix associated with the spectral channel l, and $\boldsymbol{W} = (\boldsymbol{w}_1, .., \boldsymbol{w}_L) \in \mathbb{C}^{M\times L}$ is additive white Gaussian noise. Assuming the noise has a bounded energy per block, we consider a block-wise forward model of the form $\boldsymbol{y}_{\ell,b} = \boldsymbol{\Phi}_{\ell,b}\bar{\boldsymbol{x}}_l + \boldsymbol{w}_{\ell,b}$, where $\boldsymbol{y}_{\ell,b} \in \mathbb{C}^{M_b}$ is the b-th data block in the spectral channel ℓ and $\boldsymbol{\Phi}_{\ell,b}$ is the associated measurement operator. The task of finding an estimate of $\bar{\boldsymbol{X}}$ requires solving a high dimensional ill-posed inverse problem (typically $N = 10^{14}$ and $L = 10^3$ in the context of wideband RI imaging in the new radio telescopes era) and consequently involves significant uncertainty about the true image cube. A common Bayesian approach consists in modelling $\bar{\boldsymbol{X}}$ as a random variable with log-concave prior distribution $p(\boldsymbol{X})$, and using MAP approach to define the estimate as $\boldsymbol{X}^\dagger \in \text{Argmin } f_{\boldsymbol{Y}} + g$, where $f_{\boldsymbol{Y}}(\boldsymbol{X}) = -\log p(\boldsymbol{Y}|\boldsymbol{X})$ is associated with the measurement model and $g(\boldsymbol{X}) = -\log p(\boldsymbol{X})$. In this work, data fidelity is ensured by restraining the modeled data to ℓ_2 balls $\mathcal{B}(\boldsymbol{y}_{\ell,b}, \varepsilon_{\ell,b})$ centred in $\boldsymbol{y}_{\ell,b}$ and of radius $\varepsilon_{\ell,b} > 0$, i.e. $f_{\boldsymbol{Y}}(\boldsymbol{X}) = \sum_{\ell=1}^{L}\sum_{b=1}^{B} \iota_{\mathcal{B}(\boldsymbol{y}_{\ell,b},\varepsilon_{\ell,b})}\big(\boldsymbol{\Phi}_{\ell,b}\boldsymbol{x}_l\big)$. A typical convex model for HS intensity images involves positivity and joint sparsity [2], thus we consider $g(\boldsymbol{X}) = \iota_{\mathbb{R}_+^{N\times L}}(\boldsymbol{X}) + \|\boldsymbol{\Psi}\boldsymbol{X}\|_{2,1}$, where $\|\cdot\|_{2,1}$ denotes the $\ell_{2,1}$ norm and $\boldsymbol{\Psi} \in \mathbb{R}^{D\times N}$ represents a sparsity dictionary. The last decades have witnessed the advent of many imaging algorithms which provide fast and robust MAP estimates [3], [4]. These methods provide solutions that are easily visualized, yet are typically unable to analyze the uncertainty associated with the solution delivered. UQ is a very challenging task for high dimensional inverse problems and it is becoming very important in many applications related to quantitative imaging [5], scientific inquiry, and image-driven decision-making [6]. Moreover, for highly ill-posed inverse problems, uncertainty information regarding reconstructed images (e.g. error estimates) is critical. To address this problem for HS imaging, we extend our work in [1] for single-channel UQ and propose a new hyperspectral uncertainty quantification (HSUQ) method by leveraging convex optimization techniques.

II. Hyperspectral Uncertainty Quantification

The proposed method takes the form of Bayesian hypothesis test for specific 3D structures appearing in the MAP estimate. To define the test, we postulate the following hypotheses: H_0: "The 3D structure of interest is ABSENT in $\bar{\boldsymbol{X}}$" and H_1: "The 3D structure of interest is PRESENT in $\bar{\boldsymbol{X}}$". These hypotheses split the set of images $\mathbb{R}_+^{N\times L}$ onto two regions; the set $\mathcal{S}$ denoting the region containing all images without the 3D structure, and the set $\mathcal{C}_\alpha$ representing the smallest region, including the MAP, over which the posterior integrates to $(1-\alpha)$ [7]. We formulate the Bayesian hypothesis test as a convex minimization problem $\min_{\boldsymbol{X}_{\mathcal{C}_\alpha}\in\mathcal{C}_\alpha, \boldsymbol{X}_{\mathcal{S}}\in\mathcal{S}} \|\boldsymbol{X}_{\mathcal{C}_\alpha} - \boldsymbol{X}_{\mathcal{S}}\|_F^2$, and we solve it using a scalable and fast primal-dual algorithm with forward-backward iterations [1]. For more clarity, Fig. 1 shows a simple illustration of the proposed approach.

III. Application to wideband RI imaging

We leverage the proposed method in the context of wideband RI imaging in astronomy. Following [8], we simulate a wideband RI model cube composed of $L = 15$ spectral channels from a 256×256 image of the W28 supernova remnant. The wideband RI data are generated from a realistic u-v coverage and $\boldsymbol{W}$ is a realization of a $\mathcal{N}(0, 0.1)$ distribution. We define the sampling rate as the ratio between the number of measurements per channel M and the size of the image N: SR $= M/N$. To precisely evaluate the interest of the proposed approach, we quantify the uncertainty of 3 different structures appearing in the MAP estimate, highlighted in Fig. 2, varying SR from 0.005 to 2. We report in Fig. 3 the values of the metric ρ_α[1] in percentage as a function of SR for the considered 3D structures, where ρ_α represents the minimum ascertained percentage of energy in the structure at level $(1-\alpha)$ [1]. We notice for the 3 structures that the confirmed minimum energy ρ_α naturally increases when the number of measurements increases, meaning that the structure uncertainty decreases when SR increases. This is due to the fact that the investigated structures are originally present in true image cube. Interestingly for structure 2, the hypothesis H_0 is always rejected for all the considered sampling rates. Conversely, H_0 cannot be rejected for structure 1 when SR < 0.05 and cannot be rejected for structure 3 when SR < 0.02. Also we have $\rho_\alpha > 90\%$ for structure 3 for all the considered sampling rates.

IV. Conclusion

In this work, we presented a HSUQ method relying on the recent Bayesian inference results presented in [7] and leveraging modern convex optimization techniques. The proposed method is a generalization of our previous work for single-channel UQ [1]. We investigated the interest of our approach for wideband RI imaging on realistic simulations. We emphasize on the fact that HSUQ tools are of great interest for astronomers, particularly in the era of the new generation telescopes, namely SKA, where giga-pixel sized images over thousands of frequency channels are expected.

[1] $\rho_\alpha = \|\boldsymbol{X}_{\mathcal{C}_\alpha}^\ddagger - \boldsymbol{X}_{\mathcal{S}}^\ddagger\|_F / \|\boldsymbol{X}_{\mathcal{C}_\alpha}^\dagger - \boldsymbol{X}_{\mathcal{S}}^\dagger\|_F$, where $\boldsymbol{X}_{\mathcal{C}_\alpha}^\ddagger$ and $\boldsymbol{X}_{\mathcal{S}}^\ddagger$ are the solutions obtained by the proposed approach and $\boldsymbol{X}_{\mathcal{S}}^\dagger$ corresponds to the MAP estimate $\boldsymbol{X}_{\mathcal{C}_\alpha}^\dagger$ where the 3D structure of interest has been removed.

ACKNOWLEDGEMENT

This work was supported by the UK Engineering and Physical Sciences Research Council (EP/M008843/1 and EP/M019306/1), and used the Cirrus UK National Tier-2 HPC Service at EPCC (http://www.cirrus.ac.uk) funded by the University of Edinburgh and EPSRC (EP/P020267/1).

REFERENCES

[1] A. Repetti, M. Pereyra, and Y. Wiaux, "Uncertainty quantification in imaging: When convex optimization meets bayesian analysis," in *2018 26th European Signal Processing Conference (EUSIPCO)*, Sep. 2018, pp. 2668–2672.

[2] J. A. Tropp, "Algorithms for simultaneous sparse approximation. part ii: Convex relaxation," *Signal Processing*, vol. 86, no. 3, pp. 589–602, 2006.

[3] P. L. Combettes and J.-C. Pesquet, "Proximal splitting methods in signal processing," *Fixed-Point Algorithms for Inverse Problems in Science and Engineering*, vol. 49, pp. 185–212, May 2011.

[4] N. Komodakis and J.-C. Pesquet, "Playing with duality: An overview of recent primal-dual approaches for solving large-scale optimization problems," *IEEE Signal Processing Magazine*, vol. 32, no. 6, pp. 31–54, Nov. 2015, ISSN: 1053-5888.

[5] R. Duarte, A. Repetti, P. A. Gómez, *et al.*, "Greedy Approximate Projection for Magnetic Resonance Fingerprinting with Partial Volumes," *arXiv e-prints*, Jul. 2018.

[6] A. Dabbech, A. Onose, A. Abdulaziz, *et al.*, "Cygnus A super-resolved via convex optimization from VLA data," vol. 476, no. 3, pp. 2853–2866, Apr. 2018.

[7] M. Pereyra, "Maximum-a-posteriori estimation with bayesian confidence regions," *SIAM Journal on Imaging Sciences*, vol. 10, no. 1, pp. 285–302, 2017.

[8] A. Abdulaziz, A. Dabbech, and Y. Wiaux, "Wideband super-resolution imaging in radio interferometry via low rankness and joint average sparsity models (HyperSARA)," *arXiv e-prints*, Jun. 2018.

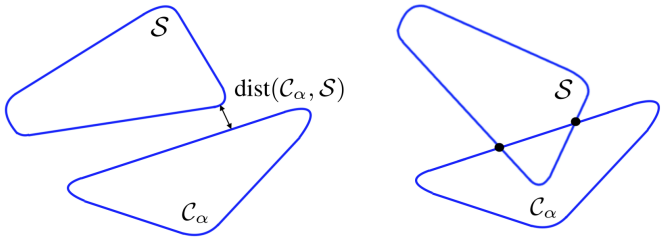

Fig. 1: Illustration of the proposed method for different scenarios. Our approach simply consists in examining the euclidean distance between the two sets $\mathcal{S}$ and $\mathcal{C}_\alpha$, i.e. $\text{dist}(\mathcal{C}_\alpha, \mathcal{S}) = \min_{\boldsymbol{X}_{\mathcal{C}_\alpha} \in \mathcal{C}_\alpha, \boldsymbol{X}_{\mathcal{S}} \in \mathcal{S}} \|\boldsymbol{X}_{\mathcal{C}_\alpha} - \boldsymbol{X}_{\mathcal{S}}\|_F^2$. Left: there is no intersection between the two sets, thus H_0 is rejected at level α. Right: the two sets intersect, thus one cannot reject H_0, i.e. one cannot conclude if the 3D structure exists in the true image cube or not.

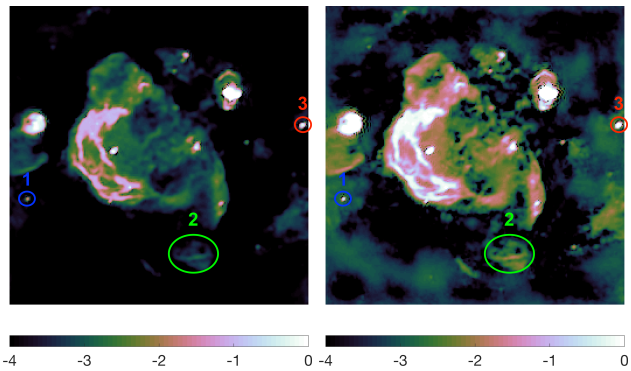

Fig. 2: First and last channels (left and right, respectively) of the W28 MAP estimate obtained considering SR $= 1$. The wideband model cube, denoted by $\bar{\boldsymbol{X}}$, is built following the linear mixture model $\bar{\boldsymbol{X}} = \bar{\boldsymbol{S}}\bar{\boldsymbol{H}}^\dagger$, where the matrix $\bar{\boldsymbol{S}} = (\bar{s}_1, .., \bar{s}_Q) \in \mathbb{R}^{N \times Q}$ represents the physical sources present in the first channel image, and their corresponding spectral signatures constitute the columns of the mixing matrix $\bar{\boldsymbol{H}} = (\bar{h}_1, .., \bar{h}_Q) \in \mathbb{R}^{L \times Q}$.

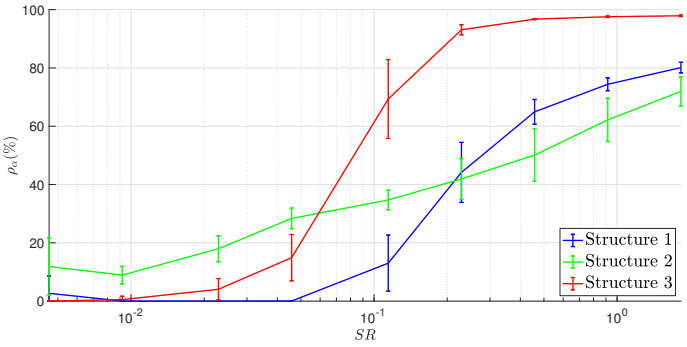

Fig. 3: Curves representing the values of ρ_α, in percentage, in log-scale, as a function of the sampling rate SR$= M/N$, for the 3 different structures of interest. In our simulations, we consider $\alpha = 1\%$ and we consider that H_0 is rejected (i.e. the structure is present) when $\rho_\alpha > 2\%$ (to allow for numerical errors). The considered 3D structures are highlighted on the first and last channels of the MAP estimate displayed in Fig. 2. Each point corresponds to the mean value of 5 tests with different antenna positions and noise realizations, and the vertical bars represents the standard deviation of 5 the tests.